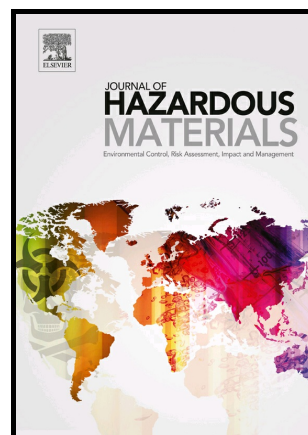


High affinity of 3D spongin scaffold towards Hg(II) in real waters

Eddy M. Domingues, Gil Gonçalves, Bruno Henriques, Eduarda Pereira, Paula A.A.P. Marques



PII: S0304-3894(20)32798-9

DOI: <https://doi.org/10.1016/j.jhazmat.2020.124807>

Reference: HAZMAT124807

To appear in: *Journal of Hazardous Materials*

Received date: 6 October 2020

Revised date: 26 November 2020

Accepted date: 6 December 2020

Please cite this article as: Eddy M. Domingues, Gil Gonçalves, Bruno Henriques, Eduarda Pereira and Paula A.A.P. Marques, High affinity of 3D spongin scaffold towards Hg(II) in real waters, *Journal of Hazardous Materials*, (2020) doi:<https://doi.org/10.1016/j.jhazmat.2020.124807>

This is a PDF file of an article that has undergone enhancements after acceptance, such as the addition of a cover page and metadata, and formatting for readability, but it is not yet the definitive version of record. This version will undergo additional copyediting, typesetting and review before it is published in its final form, but we are providing this version to give early visibility of the article. Please note that, during the production process, errors may be discovered which could affect the content, and all legal disclaimers that apply to the journal pertain.

© 2020 Published by Elsevier.

High affinity of 3D spongin scaffold towards Hg(II) in real waters.

Eddy M. Domingues^{a*}, Gil Gonçalves^{a*}, Bruno Henriques^{b,c}, Eduarda Pereira^c and Paula A. A. P. Marques^{a*}

^a - TEMA, Mechanical Engineering Department, University of Aveiro, 3810-193 Aveiro, Portugal

^b - CESAM & Department of Chemistry, University of Aveiro, 3810-193 Aveiro, Portugal

^c - LAQV-REQUIMTE, Department of Chemistry & Central Laboratory of Analysis, University of Aveiro, 3810-193 Aveiro, Portugal

Corresponding authors.

E-mail addresses: eddy@ua.pt (E.M. Domingues), ggoncalves@ua.pt (G. Goncalves), paulam@ua.pt (P. A. A. P. Marques)

Abstract

This study focuses on the ability of commercial natural bath sponges, which are made from the skeletons of marine sponges, to sorb Hg from natural waters. The main component of these bath sponges is spongin, which is a protein-based material, closely related to collagen, offering a plenitude of reactive sites from the great variety of amino acids in the protein chains, where the Hg ions can sorb. For a dose of 40 mg L⁻¹ and initial concentration of 50 µg L⁻¹ of Hg(II), marine spongin (MS) removed ~90 % of Hg from 3 water matrixes (ultrapure, bottled, and seawater), corresponding to a residual

concentration of $\sim 5 \mu\text{g L}^{-1}$, which tends to the recommend value for drinking water of $1 \mu\text{g L}^{-1}$. This value was maintained even by increasing the MS dosage, suggesting the existence of a gradient concentration threshold below which the Hg sorption mechanism halts. Kinetic modelling showed that the Pseudo Second-Order equation was the best fit for all the water matrixes, which indicates that the sorption mechanism relies most probably on chemical interactions between the functional groups of spongin and the Hg ions. This material can also be washed in HNO_3 and reused for Hg sorption, with marginal losses in efficiency, at least for 3 consecutive cycles.

Keywords: Spongin, Mercury Remediation, Real Waters, Kinetic and Equilibrium Modelling

1. Introduction

The presence of trace metals in water is a threat to the health of humans and to all forms of life. These non-biodegradable contaminants tend to bio-accumulate in the food chain, eventually reaching the human population.[1] Amongst the several trace metals found in water all over the world, Mercury (Hg(II)) is classified as the third most dangerous substance in terms of frequency, exposure risk and toxicity to human.[2] In aquatic ecosystems, the inorganic Hg tends to be converted into its toxic methyl form, $\text{Hg}(\text{CH}_3\text{Hg})$, and it can easily make its way to humans through the food chain, mainly by the ingestion of marine fish,[3]. Methyl mercury, even in trace concentration, is acutely toxic and may affect the central nervous and cardiovascular systems.[4] The presence of metallic or inorganic form of Hg in human has a harmful impact in the immune system, kidneys and lungs.[5] It is thus imperative to continue searching for

new and more efficient materials that can remove Hg from different real water matrixes. Furthermore, the United Nations has set a goal of minimizing the release of Hg, and other contaminants, which is a driving force to develop and implement new and improved remediation technologies for industrial and domestic wastewaters. The use of natural materials for this purpose is an obvious choice in terms of eco-friendliness and sustainability. In the case of Hg remediation, many examples of the use of natural, or natural-based materials can be found in the literature, including agricultural waste, such as peanut or pistachios shells,[6] onions,[7] parts of plants, such as bamboo or castor tree leaves [8], phragmites,[9] and karaya gum extract from *Sterculi Urens*,[10] *Cladophora* algae[11] or fungus, like *Agaricus macrosporus*. [12] However, all these publications have in common the use unrealistically high initial concentration of mercury (from 10 up to 1000 mg L⁻¹), which is much above the former limit of 50 µg L⁻¹ imposed to industrial wastewater discharge in Europe,[13] and the use of simple water matrixes, like ultrapure or distilled water, which are not representative for application in real-life conditions. More recently, several papers report the successful use of natural materials for Hg remediation in more realistic conditions of initial Hg concentration and water matrix complexity, such as the live algae,[14,15] the bark of *Eucalyptus globulus*[16] or even the peels of bananas.[17]

Marine sponges have been used as biomonitor for several contaminants for many years now, as they are filter feeders and are known to sorb a great variety of contaminants.[18,19] Live sponges have been widely used to detect harmful trace metals, and other contaminants, in coastal areas[20–26], while many studies have focused on marine sponge-associated bacteria for the same purpose.[27–30]. The majority of the so-called “commercial sponges”, which are sold as the bleached and cleaned skeleton of this ancestral animal, originate mainly from the Genus *Spongia* and

Hippospongia. [18] The skeletons of these species are mainly made from a protein called spongin, whose structure is still quite unknown. [31] According to Ehrlich, spongin is not a pure protein structure, but rather a type of collagen-based composite that combines with halogenated fibrillary structures and results in a compact network of nanofibrils. [19] An early study from 1939, from Block and Bolling, shows that the chemical composition of MS consists in several amino-acids, mainly Glycine (13.9-14.4%), Arginine (4.3-5.9%), Diiodotyrosine (4.7%), Lysine (3-3.6%), Phenylalanine (3.3%), and Cystine (2.8%). Naturally, there is a high amount of Nitrogen (13-14.8%) as well as Sulfur (0.7%) and Iodine (0.84-1.46%). [32] These values can fluctuate significantly between different species, even in the same Genus, as there are several types of spongin, which are basically considered to be a composite protein-based material. The microstructure of the commercial MS normally shows an anastomosed (i.e. branched) structure with an interconnected network of fibrils, which ultimately creates a 3D spongin scaffold, that supports the animal cell tissues. [18]

Although there are only few examples on the literature of the direct use of MS for remediation of pollutants (like the use of a MS from *Hippospongia Communis* used in the adsorption of Carminic Acid-C.I. Natural Red 4), [33] there are many studies that take advantage of the natural 3D scaffold of MS to incorporate or immobilize functional groups. Some examples include: the functionalization of MS with Cu or Fe(III) phthalocyanines and Ti(IV) oxide for the photocatalytic degradation of rhodamine B, bisphenol A and methylene blue, respectively, [34–36] the use of anthocyanin dye for enhanced antiradical activity, [37] a sodium and copper chlorophyllin functionalized MS substrate with antibacterial activity, [38] a poly(imide dioxime)/alginate thin film on MS substrate for the extraction of uranium in seawater, [39] immobilizing *Trametes versicolor* laccase on MS for the biodegradation of bisphenols, [40] and using MS

scaffold for the pre-concentration and determination of ketamine.[41] MS was shown to have mechanical and thermal stability (up to 160°C),[42] which enables it to be successfully applied in the recent scientific field of extreme biomimetics.[43–45] A recent paper shows an *ab initio* study in which several MS derived cyclic peptides are evaluated for their potential affinity towards Hg^{2+} and CH_3Hg^+ ions.[46]

To the best of our knowledge, MS has never been directly used for the removal of Hg from ultrapure (MQ) or real waters, which is the aim of this study. In terms of sustainability and eco-friendliness, the use of MS in its pure form is very promising. First, the virtually inexistent toxicity induced by this natural material is very advantageous. Second, the possibility of easily separating the contaminated MS sample after equilibrium from the treated water without a major time-consuming physical process involved (filtration or centrifugation) is economically sound. Third, since it is fairly easy to farm marine sponges in order to obtain MS, which is a well-established industry in several countries, it can be considered a sustainable way to procure natural 3D scaffolds for water remediation and many other applications, aiming at the valorization of natural resources. Beginning at more realistic Hg concentration ($50 \mu\text{g L}^{-1}$), and complex water matrixes, our results point out that MS samples were able to remove 91%, 90% and 89% of Hg contaminated MQ, bottled and seawater matrixes, respectively. Regeneration and reuse studies showed that MS kept a high Hg removal efficiency (R%) in all the water matrices used, even after 3 cycles.

2. Materials and methods

2.1. Preparation of the marine spongin

The bath sponges, which are bleached skeletons of marine sponge, were sourced in a local commercial facility. After being diced in cubes of approximately 1 cm³, the samples were soaked in distilled water and squeezed manually several times, renewing the water between squeezes, to remove any loose fragments and promote the release of possible salts and other contaminants. The pieces of spongin (c.a. 3 g) were then placed in a large 2 L container of distilled water and left under vigorous agitation for 24 h, drained and washed again for 24 h more. The samples were then drained and dried in vacuum oven at 50 °C for 24 h and kept in a desiccator for storage. We performed Energy-dispersive X-ray Spectroscopy (EDS) to evaluate the chemical composition of the MS samples before (as-received) and after the cleaning protocol which results are presented in the SI (Figure SI-1).

2.2. Characterization

The chemical structure of the MS was analyzed via Attenuated Total Reflectance Fourier Transform Infrared (ATR-FTIR) in a Bruker Tensor 27 FT-IR spectrometer (Bruker Corporation, Massachusetts, USA). The spectra were recorded between 4000 and 400 cm⁻¹, with a resolution of 4 cm⁻¹ and 256 scans, at 20 °C and 30% relative humidity. XPS was also used to clarify the structure of the MS and the spectra were obtained in an ultra-high vacuum system (SPECS, Berlin, Germany) using a base pressure of 2×10^{-10} mbar. The global instrumental peak broadening was of ~0.5 eV, provided by using a normal emission take-off angle with a pass energy of 20 eV. The binding energy was rectified in the spectra by referencing to the first component of the

C1s core level at 284.5 eV (Csp²). The thermogravimetric analysis/Differential Scanning Calorimetry (TGA/DSC) was performed from room temperature up to 1000 °C in a Netzsch STA 449 F3 Jupiter (Netzsch GmbH & Co, Selb, Germany), under N₂ atmosphere and 5 °C min⁻¹ heating rate. The microstructure was analysed by Scanning Electron Microscopy (SEM) using a Hitachi TM4000 plus (Hitachi, Japan) using an accelerating voltage of 15 kV. The computerized tomographic scans (CT) were performed in a Bruker Skyscan 1275 X-ray microtomography (Bruker Corporation, Massachusetts, USA) with voltage of 20 kV, 175 μA current and 450 ms exposure time.

2.3. Water matrixes preparation

In this work 3 different types of water were used: ultrapure water (MQ) from Milli-Q®, USA; 18 MΩ cm⁻¹, bottled water (commercial brand Fastio®, Portugal), and synthetic seawater (salinity 30) (prepared by dissolving salt from Tropic Marin Center®, Germany, in MQ). The use of bottle water instead of tap was to assure the consistency of the water used. The use of synthetic seawater (salinity of 30, using a hand-held refractometer) allows to have reproduceable matrix, which is normally used in several studies to assess the effect of contaminants on living organisms.[47–49] The full characterization of this synthetic seawater is comprehensibly available in the literature.[50] After the salt mix was completely dissolved, the seawater was filtered (0.45 μm pore size filter) and stored for at least 24 h prior to being used in Hg sorption experiment. The initial pH of the water matrixes after the addition of Hg contaminant was of 4.9, 5.9 and 7.8 for MQ, bottled and seawater, respectively. The full characterization of the bottled water is presented in the SI (table SI-1).

2.4. Mercury sorption studies

A standard solution of Hg ($1001 \pm 2 \text{ mg L}^{-1}$ of Hg(II) in HNO_3 0.5 mol L^{-1} , from Merck, Germany) was used to contaminate MQ, bottled, and seawater, in 1 L glass bottles (Schott, Germany), to obtain the concentration of $50 \text{ } \mu\text{g L}^{-1}$ in Hg, which is equal to the maximum allowed value for industrial wastewater discharges in Europe.[13] The contaminated waters were left for 24 h, under magnetic stirring, before being used in the sorption experiments. The sorption of Hg into MS samples was performed in batch experiments by adding $\sim 40 \text{ mg}$ of dry MS to 1 L Hg contaminated water (MQ, bottled or seawater), under magnetic stirring (700 rpm). Alongside, Hg contaminated control bottles, without any MS added, were also prepared. To study the kinetics of the sorption process, an aliquot of 5 mL was removed from the trial vessels as a function of time (0.25, 0.5, 1, 2, 3, 6, 24 and 48 h), and acidified to $\text{pH} \leq 2$ (Suprapur HNO_3 65 % v/v from Sigma, USA) in a Schott bottle (25 mL). The analysis Hg in water was performed by cold vapour atomic fluorescence spectroscopy (CV-AFS), using a PSA 10.025 Millennium Merlin Hg analyzer and SnCl_2 (2% m/v in HCl 10% v/v) as a reducing agent. After calibrating the CV-AFS using 5 standard Hg solutions (0, 0.1, 0.2, 0.3 and $0.5 \text{ } \mu\text{g L}^{-1}$), the fluorescence of the appropriately diluted aliquot was read and compared to the results from the standards slope to calculate the real concentration. All assays were conducted in duplicate and accepted values had a variation coefficient of less than 10%. The temperature range at which the experiments were performed was between 18°C and 22°C .

2.4.1. Sorption data analysis

The efficiency of the sorption process, in terms of percentage of Hg (sorbate) removed from the solution (R%) by the MS (sorbent), was calculated as:

$$R(\%) = \frac{C_0 - C_t}{C_0} \times 100 \quad (1)$$

In which C_0 is the initial concentration of the Hg solution and C_t is the Hg concentration at time t . Assuming that all the Hg removed is retained by the sorbent, the sorbate concentration in the material at time t , q_t , can be estimated as:

$$q_t = \frac{(C_0 - C_t)}{m} \times V \quad (2)$$

where V (L) is the volume of the solution and m (g) is the mass of sorbent. At equilibrium time t_e , $q_t = q_e$ and $C_t = C_e$. [51] In order to compare results between trials, the analysis of the sorption data was made using normalized concentration (C_t/C_0) because in most cases the actual initial concentration of the spiked solutions shows small deviations from the nominal initial concentration.

2.4.2. Kinetics and equilibrium models

To understand the sorption process kinetics, three reaction models, in their non-linear form, were applied to fit the experimental data, [52] namely the Lagergren pseudo-first-order model (PFO), [53] Ho's pseudo-second-order model (PSO), [54] and the Elovich model [55] (see Table SI-2 in SI for details). Additionally, two diffusion-based models were applied, namely Boyd's film-diffusion [56] and Weber's intraparticle diffusion [57] (details in SI).

Five different non-linear models were used to fit the equilibrium data, namely the Freundlich, [58] the two-parameter Langmuir, [59] the Dubinin-Radushkevich, [60] the

Temkin[58] and the 3-parameter Sips (also known as the Langmuir-Freundlich)[61] isotherm models. Please consult table SI-3 for further details.

2.4.3. Desorption of mercury and reuse of sorbent

The ability of MS to be regenerated and reused after Hg sorption was evaluated in MQ water by realizing 3 consecutive sorption/desorption cycles. For the desorption process, the MS samples used in the Hg sorption were immersed in 200 mL HNO₃ (10% v/v), under constant stirring, for 24 h to promote de desorption of the captured Hg and study its ability to be reused. After the acid bath, the samples were rinsed in abundant distilled water and stirring overnight in 1 L of distilled water and finally dried. The total amount of Hg in the MS samples (before sorption, after sorption and after regeneration) was evaluated by pyrolysis atomic absorption spectroscopy with gold amalgamation (model AMA-254, from LECO, Korea).[62] This analysis was performed directly in the MS samples (between 2 to 10 mg), defining a maximum coefficient of variation of 10% between replicas. Two certified Hg containing reference materials were used: for low Hg content BCR 414 (plankton) and for high Hg content, BCR 464 (fish muscle) and the recovery percentage was above 90 %.

3. Results and discussion

3.1. Physico-chemical characterization of sorbent material

An example of a typical bath sponge is depicted in Figure 1A. The microstructure of the sample was observed by SEM (micrograph depicted in Figure 1B), which revealed the

expected honeycomb-like structure, with anastomosed spongin fibers that ranged between 5 to 20 μm in diameter.[18,31]

XPS analysis was used to determine the chemical states of the functional groups on the surface of MS. The survey XPS (Figure 1C) shows the presence of O, N and C, as expected from the amino-acid content of spongin, and traces of Ca and Si. However, due to the overlapping of many broad peaks, from several different functional groups present in the amino acid that constitute spongin, the assignment and deconvolution of the peaks is more difficult. Nevertheless, and according to the literature, the high resolution XPS C1s spectrum suggests the presence of functional groups C=O (from N-C=O and O-C=O) at ~ 287.5 eV, C-O-C, C-OH, C-C, C=C, and N-C=N at ~ 285 eV and C-H at ~ 282 eV. In the case of the high resolution XPS N 1s spectrum, the analysis suggest the presence of the functional groups C-N at ~ 398 eV, $-\text{NH}_2$ at ~ 400 eV and C=N at ~ 401 eV.[33,35,63,64]

The thermal analysis of the MS, performed in N_2 atmosphere, shows 3 stages of thermal decomposition, as observable in Figure 1D. The first step (up to ~ 115 $^\circ\text{C}$) can naturally be associated to the loss of adsorbed water from the structure. The second step (from ~ 200 $^\circ\text{C}$ to 400 $^\circ\text{C}$) is a steep mass loss that can be mostly linked to the degradation of the organic phase of the spongin protein.[33,37]. The last step of mass loss (400 $^\circ\text{C}$ and onward) corresponds to a slower loss of mass and can be associated to the on ongoing degradation of the protein backbone and to the combustion of the organic matrix of spongin, much similarly to bovine bone collagen.[65]

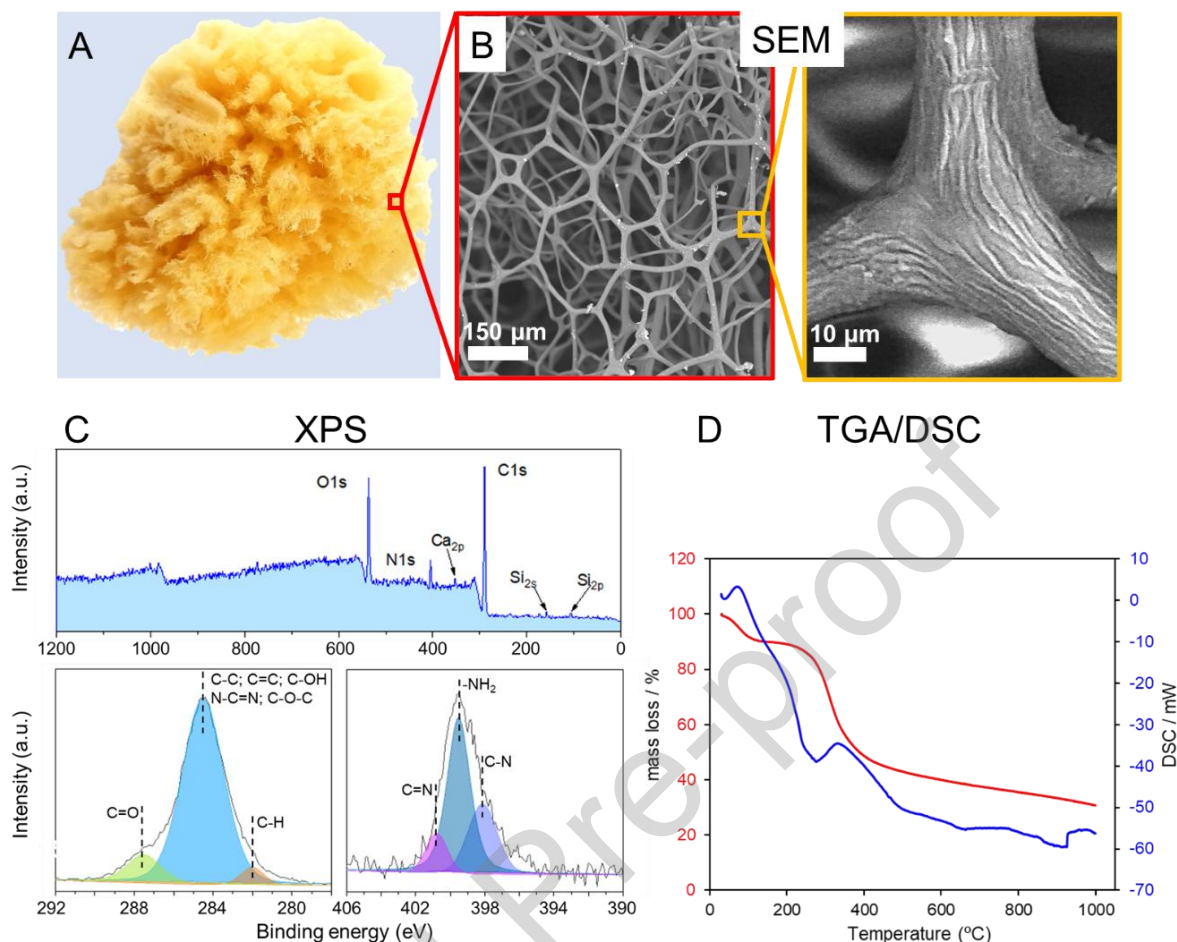


Figure 1. A) Photograph of a typical marine sponge skeleton, or commercial bath sponge, used in this work. B) SEM micrograph showing the microstructure of the MS. C) Survey XPS and detailed high-resolution XPS for C 1s and N 1s. D) TGA/DSC scan of MS sample.

Spongin is considered a protein composite, [19] and as such, FTIR spectra (Figure 2) will present broad, strong bands, with substantial overlap, which make them difficult to distinguish. Hence, the broad peaks in the $3600\text{-}3100\text{ cm}^{-1}$ interval can be attributed to N-H stretching vibrations, including the amide A band, and to O-H stretching vibrations.[36] Stretching vibrations of -CH, -CH₂ and -CH₃ can be ascribed to the peaks in the $2950\text{-}2850\text{ cm}^{-1}$ range. The peak at $\sim 1630\text{ cm}^{-1}$ originates from stretching

vibrations of the C=O group. The peak at $\sim 1520\text{ cm}^{-1}$ can be attributed to the characteristic CO-NH, present in all protein chains. A peak at $\sim 1440\text{ cm}^{-1}$ confirms the presence of aromatic ring bearing amino-acids ($C_{ar}=C_{ar}$). The band centered at $\sim 1388\text{ cm}^{-1}$ can be assigned to $-\text{CH}_3$ deformation vibration. The bands at ~ 1020 and $\sim 1070\text{ cm}^{-1}$ can be attributed to the C-OH stretching vibrations while the band at $\sim 1230\text{ cm}^{-1}$ correspond to the C-O-C stretching but may also be connected to C-N stretching. The broad peak centered around 550 cm^{-1} can be assigned to O=C-N or to -OH bending vibrations.[33,37,64] The results observed by the FTIR analysis confirms the functional groups detected in the XPS analysis presented previously.

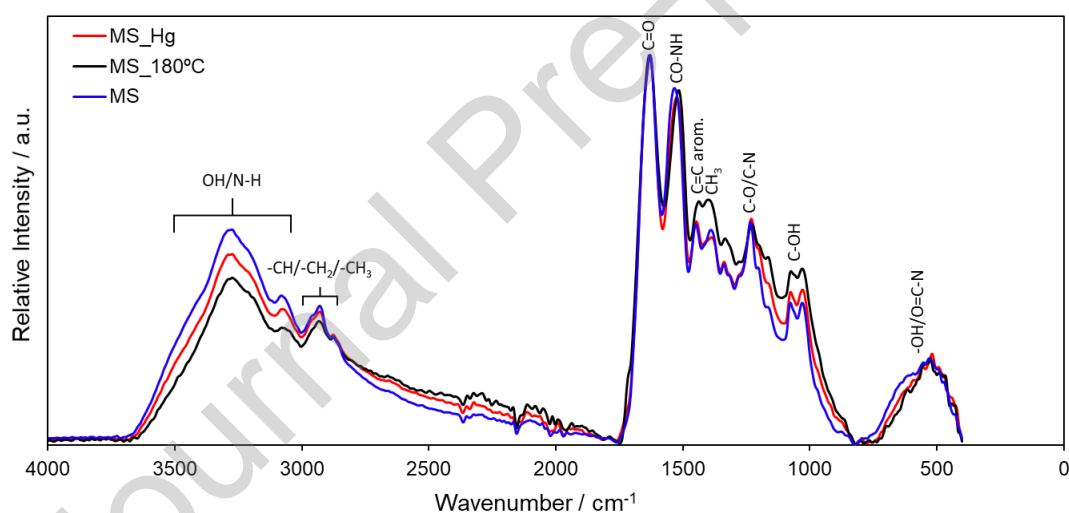


Figure 2. FTIR spectra of MS samples as received, heat-treated at 180°C and after contact with Hg solution.

To increase the stiffness of the MS, which would increase its ability to withstand mechanical stress and extend its use in harsh conditions, namely in highly stirred media, the spongin was heat-treated in a vacuum oven overnight. Based on the observations made in the thermogravimetric analysis, the temperature of 180°C was chosen for this treatment, i.e. just before the observed decomposition of the organic phase. In fact, a dry

mechanical analysis revealed an increase in the Young Modulus of MS from 120 kPa at room temperature to 270 kPa at 180°C (Figure SI-2 in the SI). The sample was observed by CT scan before and after the heat treatment at 180 °C, and the comparative images are presented in Figure 3. There was an irreversible color change, from bright yellow to a dark gold/brown color, with increasing temperature. Moreover, a significant volume shrinkage from untreated MS to 180°C heat-treated ($\sim 1.73 \text{ cm}^3$ down to $\sim 1.17 \text{ cm}^3$) was observed and the CT scan shows what seems to be a densification of the MS fibrils. The calculated volume of open pore space went from 85.2 % down to 51.6%. However, the FTIR analysis (Figure 3) does not show significant changes with respect to the pristine MS.

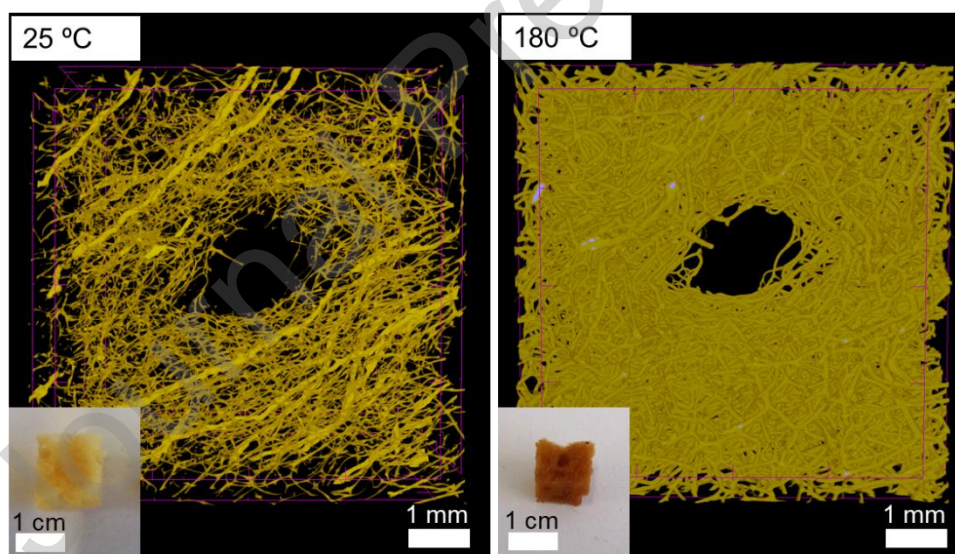


Figure 3. Photograph and CT scan of a sample of MS before and after heat-treatment at 180 °C.

3.2. Mercury sorption studies

The study of the ability of MS to sorb Hg was initiated by a series of preliminary experiments, namely a study of the effect of initial Hg concentration for the same MS

dosage (40 mg L^{-1}), as shown in Figure 4A. The MS samples in contact with a MQ water solution at 50 and $500 \text{ } \mu\text{g L}^{-1}$ of Hg showed a high R% of 91 and 94 %, respectively, which corresponds to a residual concentration of ~ 5 and $\sim 31 \text{ } \mu\text{g L}^{-1}$ of Hg in solution, respectively. This shows that, depending on the initial Hg concentration, the R% of Hg does not change a lot, but the final residual concentration may still remain very high, which reinforces the awareness that this type of sorption experiments should definitely be made in more representative conditions (i.e. $50 \text{ } \mu\text{g L}^{-1}$) and not at unrealistically high concentrations, as it is found in so many examples in the literature.[6–12]

The effect of MS concentration, or dosage, in the removal of Hg in spiked MQ water (Hg concentration of $50 \text{ } \mu\text{g L}^{-1}$) was also evaluated (Figure 4B). The R% of Hg ranged 87-91%, from a MS dosage of 40 mg L^{-1} up to 160 mg L^{-1} . The relative independence of Hg R% from MS dosage suggests that the driving force for the sorption is more dependent on the concentration gradient, with an apparent threshold at $\sim 5 \text{ } \mu\text{g L}^{-1}$ of Hg. Therefore, the dosage of 40 mg L^{-1} was selected for the remainder of the study.

The sorption ability of the heated-treated MS sample was unfortunately lower than the pristine MS (R% of 75%) as shown in Figure 4C. Although, the FTIR spectra of the heat-treated MS (Figure 2) does not reveal significant chemical changes, as shown in other studies,[42] the relative intensity of the bands in the range of $2900\text{-}3600 \text{ cm}^{-1}$ are lower than the pristine one, which can be attributed to a new reconfiguration of the MS macrostructure, as observed by the densification of the fibrils (Figure 3), which limits the availability of free amine functional groups on the surface, hindering the sorption ability of the MS.

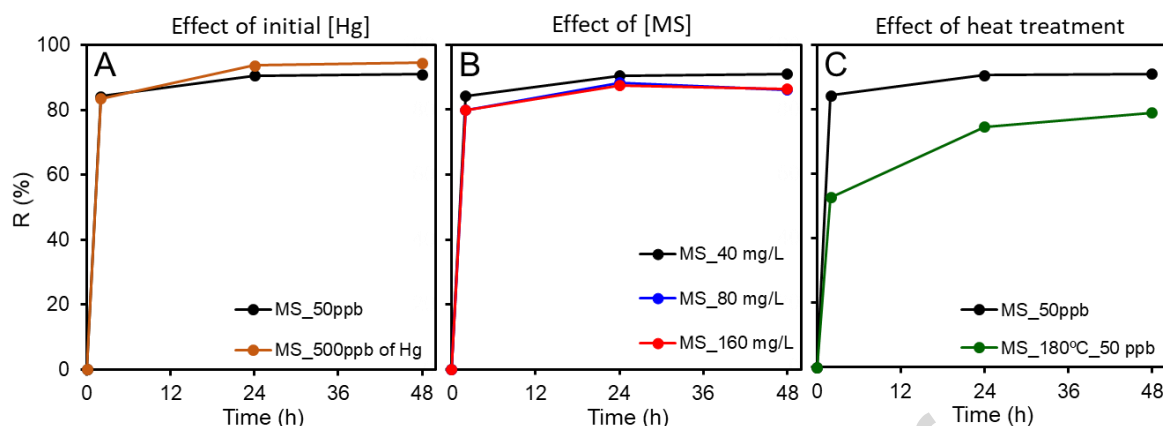


Figure 4. A) Effect of initial Hg concentration on sorption efficiency (initial MS dosage of 40 mg L^{-1}). B) Effect of increasing MS dosage on the sorption efficiency (initial Hg concentration of $50 \mu\text{g L}^{-1}$). C) Effect of MS thermal treatment at 180°C on sorption efficiency (initial Hg concentration of $50 \mu\text{g L}^{-1}$).

The dosage of 40 mg L^{-1} was selected as the most suitable for the sorption of Hg by the MS samples and it was used to evaluate the sorption of Hg for 3 different types of waters (MQ, bottled and sea). Parallely, MS-free water matrixes were also analyzed as a control. The normalized concentration (C_t/C_0), as function of time, and the maximum R% at equilibrium are depicted in Figure 5. As observable in Figure 5A, the concentration of the control vessels did not vary significantly over the period of contact, which is indicative that the decrease in Hg concentration in the vessels with MS was not due to adsorption on the glass walls or to volatilization. The efficiency of the Hg adsorption process in all the water matrixes was similar, with a R% of 91, 90 and 89% at equilibrium for MQ, bottled and seawater respectively. This corresponds to residual Hg concentration of 4.4 , 4.6 and $5.3 \mu\text{g L}^{-1}$, for MQ, bottled and seawater, respectively. The residual Hg concentration values, which tend to the European guideline for drinking water of $1 \mu\text{g L}^{-1}$, [66] are very promising, principally because this is a

completely natural material, used as is, without any physical or chemical functionalization. Table 1 is a compilation of some of the few examples found in the literature (to the best of our knowledge) that could directly compare to the application conditions presented in this paper, that is, the use of real water matrixes and Hg initial concentration of $50 \mu\text{g L}^{-1}$. Banana peel were turned into a powder and showed to remove more than 90 R% of Hg in tap and sea water after 72 h of contact.[17] Eucalyptus bark was also tested but did not show such efficient results.[16] A series of live algae also showed very promising results (85-98 R%), even in the presence of other metals and rare earths. [14,15] In terms of dosage, in our case a considerably lower dosage of sorbent (40 mg L^{-1}) could yield R% of 89 % in seawater. Also, through the kinetic profile, one can suppose that this value could increase with higher contact time.

Table 1. Removal percentage of Hg reported in published works using natural materials in similar conditions to this work.

Material	% R	Conditions	Contact time (h)	Dosage (g L^{-1})	Reference
Banana peel	91	tap	72	0.5	[17]
	93	sea	72	0.5	
Eucalyptus bark	81	MQ	48	0.55	[16]
	71	sea	48	0.5	
<i>Ulva lactuca</i> algae	98	sea (multimetal)	48	6	[14]
<i>Ulva lactuca</i> algae	93	sea (multimetal and rare earths)	72	3	[15]
<i>Ulva intestinalis</i> algae	93	sea (multimetal and rare earths)	72	3	[15]
<i>Fucus vesiculosus</i> algae	85	sea (multimetal and rare earths)	72	3	[15]
Marine Spongin	91	MQ	24	0.04	This work
	90	tap	48	0.04	
	89	sea	48	0.04	

The rate at which Hg is removed from the water matrixes is progressively slower moving from MQ to bottled water and subsequently to seawater, with equilibrium attained after 24 h for MQ and 48 h for bottled and seawater. This indicates that the adsorption process must be negatively affected by the increasing complexity of the water matrix tested.

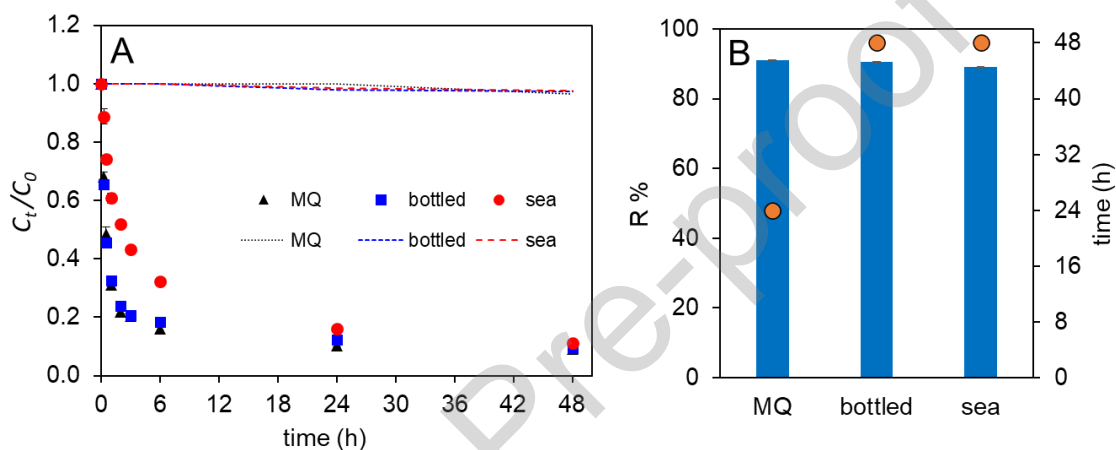


Figure 5. A) Normalized concentrations (C_t/C_0) of Hg in the water matrixes studied (symbols) and Hg in control (dotted lines), as a function of contact time; B) Efficiency of Hg removal using the MS for spiked water matrixes at equilibrium (bars) and equilibrium time (circles). MS concentration of 40 mg L^{-1} and Hg C_0 of $50 \text{ } \mu\text{g L}^{-1}$. The values are a mean of two replicates that showed a variation coefficient lower than 10 %.

3.3. Kinetic modeling

The experimental values for Hg sorbed onto MS in the different matrixes are represented in Figure 6 next to the estimated values retrieved from the adjustments made by applying the kinetic models PFO, PSO and Elovich. The parameters resulting from the fitting are exposed in Table 2. Overall, the sorption of Hg onto MS samples is

quite well described by the PFO and PSO models ($0.961 < R^2 < 0.992$). Analysing the data further, it is noticeable that the model that best fits the experimental data is the PSO, with the highest R^2 values (all above 0.99) and the estimated q_e is closer to the experimental values for all the water matrixes (less than 0.9% of relative error). The fact that the best fit is accomplished by PSO model suggests that the sorption mechanism relies most probably on chemical interactions between the functional groups of the spongin fibrils and the Hg ions.[54,67]

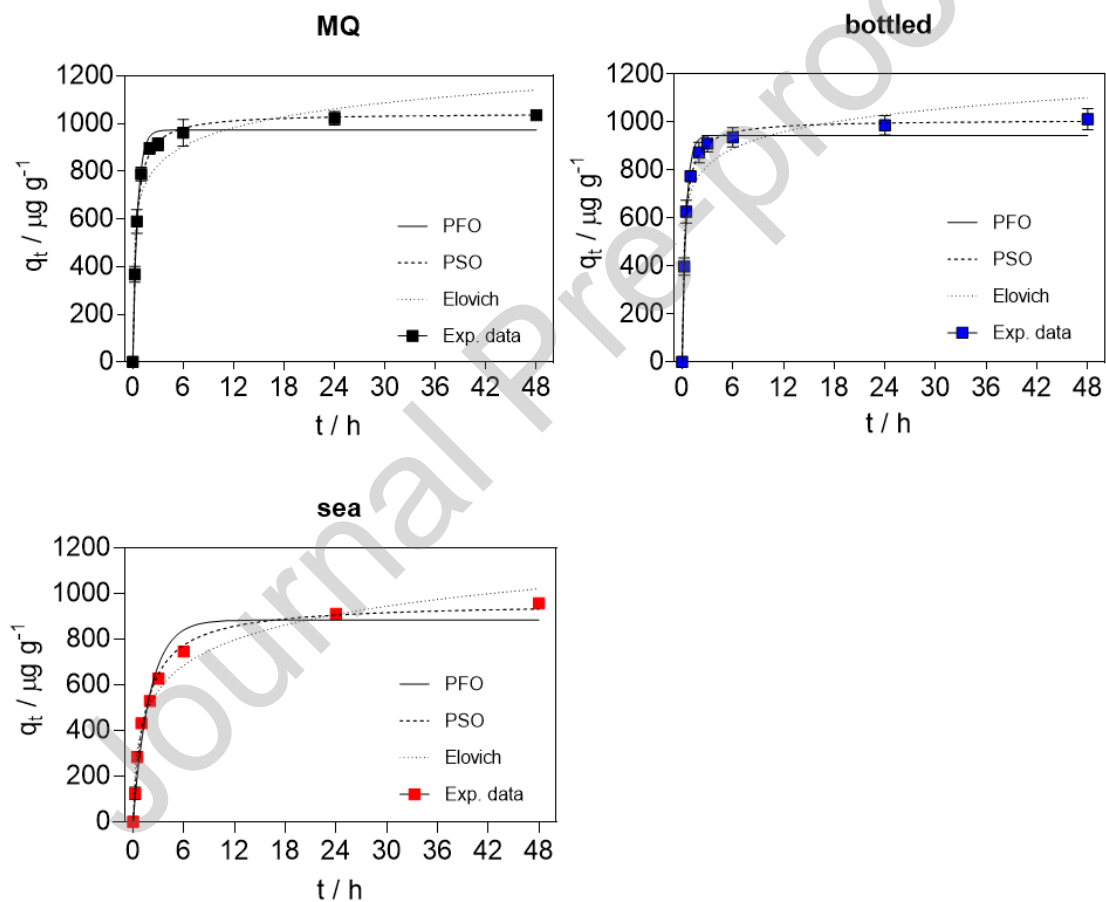


Figure 6. Experimental values of the Hg concentration in the MS samples (q_t in $\mu\text{g g}^{-1}$) and fittings using kinetic models PFO, PSO and Elovich for the different types of water matrixes.

In order to gain more information into the possible mechanism that governs the adsorption of Hg ions onto MS, a piecewise linear regression (PLR) was used to clarify the rate-controlling step.[68] This analysis was based on the film-diffusion model from Boyd[56] and the intraparticle-diffusion model from Weber.[57] The application of Boyd's model showed that in all the matrixes used, the first linear segment includes the origin, which is an indication that the rate-defining step is most probably not the film-diffusion as expected since the systems water-MS were under constant agitation.[69–71]

Table 2. Fitting parameters of the kinetic models (PFO, PSO and Elovich) used to fit the experimental data. The experimental q_e was added for comparison.

Models	Water matrices		
	MQ	bottled	sea
$q_{e1} \text{ exp} \pm \text{SD} (\mu\text{g g}^{-1})$	1034 ± 20.8	1012 ± 44.4	956.3 ± 5.1
Pseudo First Order			
$q_{e1} \pm \text{SD} (\mu\text{g g}^{-1})$	972.6 ± 15.7	945.4 ± 16.1	883.8 ± 29.5
$k_1 \pm \text{SD} (\text{h}^{-1})$	1.77 ± 0.13	2.02 ± 0.16	0.50 ± 0.05
R^2	0.981	0.978	0.961
Sy.x	47.5	49.9	66.4
Pseudo Second Order			
$q_{e2} \pm \text{SD} (\mu\text{g g}^{-1})$	1044 ± 13.7	1010 ± 13.1	960.1 ± 15.3
$k_2 \pm \text{SD} (\text{h}^{-1})$	0.0025 ± 0.0002	0.0029 ± 0.0002	$0.0007 \pm 5.2e^{-5}$
R^2	0.991	0.990	0.993
Sy.x	33.7	33.1	28.7
Elovich			
$\beta \pm \text{SD} (\text{g } \mu \text{g}^{-1})$	0.0088 ± 0.0012	0.0098 ± 0.0013	0.0062 ± 0.0004
$\alpha \pm \text{SD} (\mu\text{g g}^{-1} \text{h}^{-1})$	52678 ± 44784	100144 ± 95803	1825 ± 352.1
R^2	0.917	0.924	0.976
Sy.x	101.3	92.7	51.6

In the case of the Weber intraparticle-diffusion model, the Akaike Information Criteria (AIC)[52] was used to determine how many segments fit better the experimental data, showing that the two-segment hypothesis is more likely to be correct, which indicates

that the sorption process is most likely a two-step process, for all the water matrixes used (Figure 7). Table SI-4 has a compilation of the kinetics parameters obtained from this study. The first linear section is related to a faster diffusion driven by the higher concentration gradient, corresponding most likely to the diffusion in the larger pores of MS. The much less steep second section of the plot indicates that the intraparticle-diffusion decreases with the concentration gradient.

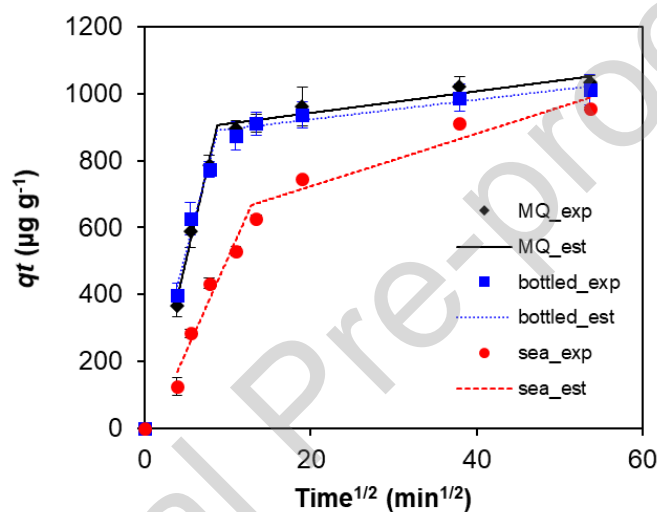


Figure 7. Results from the Weber intraparticle-diffusion model for the matrixes used, showing the two-step best fit (lines). The full symbols correspond to the experimental data.

XPS analysis could be useful to further elucidate the mechanism by which the Hg sorption takes place, but it was not possible to detect any evidence of Hg in the XPS spectra survey. This is most probably due to several factors, including the low concentration of Hg which is most probably lower than the detection limit of the XPS and the fact that XPS only penetrates only few nanometers of the surface of this highly porous material. Nevertheless, there was evidence of Hg in MS samples after contact

detected by pyrolysis atomic absorption spectroscopy with gold amalgamation (LECO). XPS revealed the presence of -NH_2 and -COOH rich amino acids in the structure of spongin, much as in the case of polyethyleneimine functionalized graphene oxide,[67] which can lead to the assumption that these groups take part in the adsorption of Hg, mainly in the form of Hg(OH)_2 , which is the main speciation form in such water matrixes,[72] through chemical interactions, as predicted by the application of the kinetic models. Figure 8 is a graphical representation of a possible interaction between Hg and MS. Furthermore, the relative intensity of the bands in the range of $2900\text{-}3600\text{ cm}^{-1}$ of the FTIR spectra (Figure 2) is lower for the MS after contact with Hg solution, which can also be an indication that these sites are occupied with Hg.

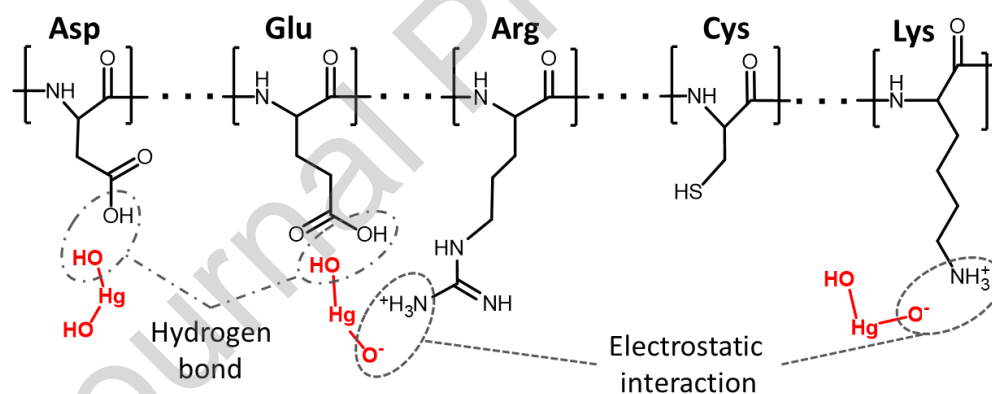


Figure 8. Schematic representation of the illustrative combination of typical amino acids found in spongin and the possible interactions with the Hg ions in solution.

3.4. Sorption isotherms

The fittings accomplished by the isotherm models, in their nonlinear forms, for the equilibrium data matching Hg sorption on the marine sponge (ultrapure water) are

shown in Figure 9, while the models parameters and the goodness of fit are presented in Table 3.

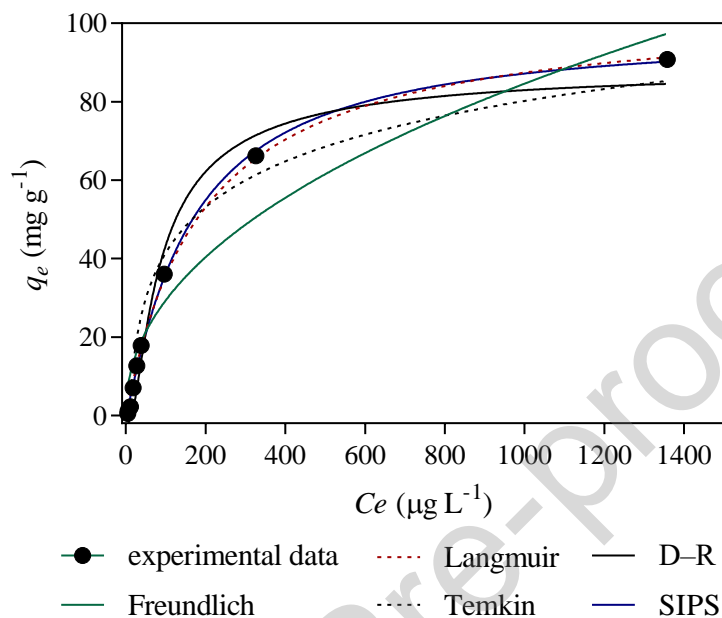


Figure 9. Isotherms (Freundlich, Langmuir, Temkin, Dubinin–Radushkevich and SIPS models) for the Hg sorption onto MS (21 ± 1 °C). Concentration of MS in ultrapure water 40 mg L^{-1} ; and of Hg 0, 25, 50, 100, 300, 500, 750, 1500, 3000 and $5000 \text{ } \mu\text{g L}^{-1}$.

Apart from the Freundlich isotherm, that was unable to describe the equilibrium data for q_e values higher than 20 mg g^{-1} , all isotherms models studied provided very reasonable fittings, for the conditions assessed, with $R^2 \geq 0.954$. Langmuir and SIPS isotherms were the models with the best performance (Table 3), being the only ones capable of describing the experimental data for higher sorbate concentrations (Figure 9). Even if SIPS adjustment achieved the highest R^2 value and the lowest $Sy.x$ value, Akaike's Information Criterion [52] pointed the simpler Langmuir model as the most likely to be the correct (79% of probability). This is in line with the heterogeneity index ($1/n$) derived from the SIPS isotherm, whose 95 % confidence interval includes 1 (0.975 to 1.27), reducing this model to the Langmuir isotherm equation, which indicates a

monolayer sorption process.[58] According to the Langmuir separation factor, R_L ($R_L=1/(1+b_L C_0)$), the adsorption is favourable for the range of concentrations studied, 25 to 5000 $\mu\text{g L}^{-1}$, varying from 0.89 to 0.040, respectively.[73] Langmuir maximum sorption capacity estimated for the MS, q_m , was within the interval 97.8 to 111 mg g^{-1} , which is very similar to that obtained by for Graphene Oxide/Polyethyleneimine aerogel (90.3 – 106 mg g^{-1}),[67] evidencing the potential of the present material, even more considering that it is a natural material, without any chemical modification.

Table 3. Isotherms parameters and goodness of fit (Freundlich, Langmuir, Temkin, Dubinin–Radushkevich and SIPS models) for the Hg sorption onto MS.

Isotherm model	Best fit values	Goodness of fit
Freundlich	K_F (95% CI), $\mu\text{g g}^{-1}$ 3.54 (1.23 to 7.38)	R^2 0.933
	$1/n$ (95% CI) 0.46 (0.34 to 0.61)	Sy.x 8.95
Langmuir	q_m (95% CI), $\mu\text{g g}^{-1}$ 104 (97.8 to 111)	R^2 0.997
	b_L (95% CI), $\text{L } \mu\text{g}^{-1}$ 0.005 (0.004 to 0.006)	Sy.x 1.99
Temkin	B (95% CI), J mol^{-1} 148 (123 to 184)	R^2 0.954
	K_t (95% CI), $\text{L } \mu\text{g}^{-1}$ 0.12 (0.08 to 0.20)	Sy.x 7.43
Dubinin–Radushkevich	q_m (95% CI), $\mu\text{g g}^{-1}$ 89.2 (77.6 to 102)	R^2 0.977
	B (95% CI), mmol^2/J^2 0.015 (0.102 to 0.022)	Sy.x 5.20
SIPS	q_m (95% CI), $\mu\text{g g}^{-1}$ 98.8 (91.7 to 108)	R^2 0.998
	$1/n$ (95% CI) 1.11 (0.08 to 1.27)	Sy.x 1.67
	b_s (95% CI) 0.006 (0.005 to 0.008)	

CI - Confidence interval

3.5. Regeneration and reuse of sorbent material

The regeneration and reuse of MS, which is an important aspect of any sorbent in terms of sustainability and economic viability, was carried out for all the water matrixes, using an initial MS load of 40 mg L^{-1} and Hg concentration of 50 $\mu\text{g L}^{-1}$. After the sorption experiment (24 hours), the MS were regenerated using a 10% (v/v) HNO_3 solution. The experiments were repeated 2 times, for a total of 3 consecutive sorption/desorption

cycles. The concentration of Hg associated with the MS, before and after regeneration, was evaluated by pyrolysis atomic absorption spectroscopy with gold amalgamation (LECO). The initial amount of Hg in the pristine MS (μg of Hg per g of MS) was found to be of $0.22 \pm 0.04 \mu\text{g g}^{-1}$. Right after Hg sorption, the sample was dried and lyophilized, and the amount of Hg present in the MS samples was found to be $575 \pm 18.7 \mu\text{g g}^{-1}$.

Figure 10 represents (in blue) the efficiency of Hg removal after the 3 regeneration/reuse cycles, in the 3 different water matrixes. There is an observable reduction in R% for the consecutive cycles, more obvious for the sample used in the seawater experiment (R% of 85 % in the first cycle down to 75 % in the third). In the same figure but in red, the results from the LECO analysis for the residual Hg % in the MS samples after the regeneration cycles is also presented. There is still a considerable amount of Hg in the samples (maximum detected of $22.9 \mu\text{g g}^{-1}$) when compared to the initial residual value of $0.22 \mu\text{g g}^{-1}$ of the pristine MS. Despite not being perfect, the regeneration method is still quite efficient (over 96 % recovery).

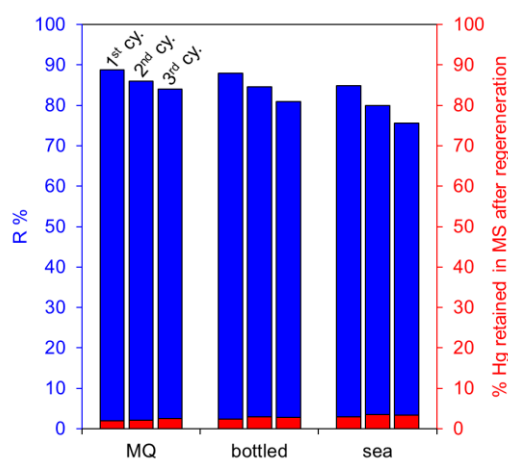


Figure 10. (Blue) Efficiency of Hg sorption (R%) for an initial MS load of 40 mg g^{-1} and initial Hg concentration of $50 \mu\text{g g}^{-1}$ in 3 different water matrixes, for 3 consecutive

cycles. The samples were washed/regenerated in 10% HNO₃ between cycles. (Red) % of retained Hg inside dry MS after regeneration.

4. Conclusion

This study shows that a naturally occurring material, spongin, which is the main component of the skeleton of common marine sponges from the genus *Spongia* and *Hippospongia*, is a great sustainable and eco-friendly candidate for the adsorption of Hg from contaminated real waters. With a starting dosage of 40 mg L⁻¹ of MS in relatively low, albeit realistic, concentration of Hg (50 µg L⁻¹), MS was able to remove 91, 90 and 89 % of Hg from MQ, bottled, and seawater, respectively. The kinetic analysis of the data revealed a best fit for the pseudo-second order equation, with R^2 over 0.99 for all water matrixes, which suggests that the chemical interactions between the functional groups of the spongin fibrils and the Hg ions must regulate the sorption mechanism. The best application of Weber's intraparticle-diffusion model was for a two-segment fit, where the first linear section is most probably related to a faster diffusion in the larger pores of MS samples, driven by the higher concentration gradient, and the second step indicates that the intraparticle-diffusion decreases with decreasing concentration gradient.

Starting at with a Hg concentration of 50 µg L⁻¹, the residual value of ~5 µg L⁻¹ in seawater is encouraging, and tends to the recommend value for drinking water of 1 µg L⁻¹. This naturally preformed 3D structure has the potential to be used as a support or immobilization scaffold for known, otherwise loose and highly dispersible, materials with high affinity to Hg, where a synergetic effect could increase the potential of both materials to sorb Hg from real waters.

Acknowledgments

We thank Portuguese Science Foundation, I.P., (FCT) for: Gil Gonçalves for Programme Stimulus of Scientific Employment – Individual Support (CEECIND/01913/2017); Bruno Henriques for a Research position funded by national funds (OE), in the scope of the framework contract foreseen in the numbers 4, 5 and 6 of the article 23 of the Decree-Law 57/2016, of August 29, changed by Law 57/2017, of July 19. Thanks, are also due for the financial support to the H₂OValue project (PTDC/NAN-MAT/30513/2017) also supported by FCT/MEC through national funds, and the co-funding by the FEDER, within the PT2020 Partnership agreement and Compete 2020 (CENTRO-01-0145-FEDER-030513). The financial support to TEMA (UIDB/00481/2020 and UIDP/00481/2020), to REQUIMTE (UIDB/50006/2020) and to CESAM (UIDB/50017/2020 and UIDP/50017/2020) is also acknowledge, as well as to CENTRO-01-0145-FEDER-022083.

References

- [1] S. Chowdhury, M.A.J. Mazumder, O. Al-Attas, T. Husain, Heavy metals in drinking water: Occurrences, implications, and future needs in developing countries, *Sci. Total Environ.* 569–570 (2016) 476–488.
<https://doi.org/10.1016/j.scitotenv.2016.06.166>.
- [2] ATDSR, Priority list of hazardous substances, (2017).
<https://www.atsdr.cdc.gov/spl/> (accessed May 20, 2020).
- [3] L.T. Budnik, L. Casteleyn, Mercury pollution in modern times and its socio-medical consequences, *Sci. Total Environ.* 654 (2019) 720–734.
<https://doi.org/10.1016/j.scitotenv.2018.10.408>.
- [4] B. Fernandes Azevedo, L. Barros Furieri, F.M.I. Peçanha, G.A. Wiggers, P.

- Frizera Vassallo, M. Ronacher Simões, J. Fiorim, P. Rossi De Batista, M. Fioresi, L. Rossoni, I. Stefanon, M.J. Alonso, M. Salaices, D. Valentim Vassallo, Toxic effects of mercury on the cardiovascular and central nervous systems, *J. Biomed. Biotechnol.* 2012 (2012). <https://doi.org/10.1155/2012/949048>.
- [5] A.S. Ayangbenro, O.O. Babalola, A new strategy for heavy metal polluted environments: A review of microbial biosorbents, *Int. J. Environ. Res. Public Health.* 14 (2017). <https://doi.org/10.3390/ijerph14010094>.
- [6] I. Anastopoulos, I. Pashalidis, A. Hosseini-Bandegharai, D.A. Giannakoudakis, A. Robalds, M. Usman, L.B. Escudero, Y. Zhou, J.C. Colmenares, A. Núñez-Delgado, É.C. Lima, Agricultural biomass/waste as adsorbents for toxic metal decontamination of aqueous solutions, *J. Mol. Liq.* 295 (2019) 111684. <https://doi.org/10.1016/j.molliq.2019.111684>.
- [7] P. Balderas-Hernández, G. Roa-Morales, M.T. Ramírez-Silva, M. Romero-Romo, E. Rodríguez-Sevilla, J.M. Esparza-Schulz, J. Juárez-Gómez, Effective mercury(II) bioremoval from aqueous solution, and its electrochemical determination, *Chemosphere.* 167 (2017) 314–321. <https://doi.org/10.1016/j.chemosphere.2016.10.009>.
- [8] I. Anastopoulos, A. Robalds, H.N. Tran, D. Mitrogiannis, D.A. Giannakoudakis, A. Hosseini-Bandegharai, G.L. Dotto, Removal of heavy metals by leaves-derived biosorbents, *Environ. Chem. Lett.* 17 (2019) 755–766. <https://doi.org/10.1007/s10311-018-00829-x>.
- [9] M.H. Raza, A. Sadiq, U. Farooq, M. Athar, T. Hussain, A. Mujahid, M. Salman, *Phragmites karka* as a biosorbent for the removal of mercury metal ions from aqueous solution: Effect of modification, *J. Chem.* 2015 (2015).

- <https://doi.org/10.1155/2015/293054>.
- [10] V.T.P. Vinod, R.B. Sashidhar, N. Sivaprasad, V.U.M. Sarma, N. Satyanarayana, R. Kumaresan, T.N. Rao, P. Raviprasad, Bioremediation of mercury (II) from aqueous solution by gum karaya (*Sterculia urens*): A natural hydrocolloid, *Desalination*. 272 (2011) 270–277. <https://doi.org/10.1016/j.desal.2011.01.027>.
- [11] J.G. Mokone, H. Tutu, L. Chimuka, E.M. Cukrowska, Optimization and Characterization of *Cladophora* sp. Alga Immobilized in Alginate Beads and Silica Gel for the Biosorption of Mercury from Aqueous Solutions, *Water, Air, Soil Pollut.* 229 (2018). <https://doi.org/10.1007/s11270-018-3859-1>.
- [12] M.J. Melgar, J. Alonso, M.A. García, Removal of toxic metals from aqueous solutions by fungal biomass of *Agaricus macrosporus*, *Sci. Total Environ.* 385 (2007) 12–19. <https://doi.org/10.1016/j.scitotenv.2007.07.011>.
- [13] Commission regulation, Directive 84/156/EEC (1984). Council Directive 84/156/EEC of 8 March 1984 on limit values and quality objectives for mercury discharges by sectors other than the chlor-alkali electrolysis industry, *Off. J. Eur. Communities*. 74 (1984) 29. <https://eur-lex.europa.eu/LexUriServ/LexUriServ.do?uri=CONSLEG:2006R1881:20100701:EN:PDF>.
- [14] B. Henriques, A. Teixeira, P. Figueira, A.T. Reis, J. Almeida, C. Vale, E. Pereira, Simultaneous removal of trace elements from contaminated waters by living *Ulva lactuca*, *Sci. Total Environ.* 652 (2019) 880–888. <https://doi.org/10.1016/j.scitotenv.2018.10.282>.
- [15] E. Fabre, M. Dias, M. Costa, B. Henriques, C. Vale, C.B. Lopes, J. Pinheiro-Torres, C.M. Silva, E. Pereira, Negligible effect of potentially toxic elements and

- rare earth elements on mercury removal from contaminated waters by green, brown and red living marine macroalgae, *Sci. Total Environ.* 724 (2020).
<https://doi.org/10.1016/j.scitotenv.2020.138133>.
- [16] E. Fabre, C. Vale, E. Pereira, C.M. Silva, Experimental measurement and modeling of Hg(II) removal from aqueous solutions using *Eucalyptus globulus* bark: Effect of pH, salinity and biosorbent dosage, *Int. J. Mol. Sci.* 20 (2019).
<https://doi.org/10.3390/ijms20235973>.
- [17] E. Fabre, C.B. Lopes, C. Vale, E. Pereira, C.M. Silva, Valuation of banana peels as an effective biosorbent for mercury removal under low environmental concentrations, *Sci. Total Environ.* 709 (2020) 135883.
<https://doi.org/10.1016/j.scitotenv.2019.135883>.
- [18] T. Jesionowski, M. Norman, S. Zóltowska-Aksamitowska, I. Petrenko, Y. Joseph, H. Ehrlich, Marine spongin: Naturally prefabricated 3D scaffold-based biomaterial, *Mar. Drugs.* 16 (2018) 1–23. <https://doi.org/10.3390/md16030088>.
- [19] H. Ehrlich, Marine biological materials of Invertebrate origin, in: *Mar. Biol. Mater. Invertebr.*, Springer, Cham, 2019: pp. 161–272.
<https://doi.org/10.1007/978-90-481-9130-7>.
- [20] T. Perez, J. Vacelet, P. Rebouillon, In situ comparative study of several Mediterranean sponges as potential biomonitors for heavy metals, *Boll. Mus. Ist. Biol. Univ. Genova.* 68 (2004) 517–525.
<http://scholar.google.com/scholar?hl=en&btnG=Search&q=intitle:IN+SITU+COMPARATIVE+STUDY+OF+SEVERAL+MEDITERRANEAN+SPONGES+AS+POTENTIAL+BIOMONITORS+OF+HEAVY+METALS#0>.
- [21] E. Cebrian, R. Martí, J.M. Uriz, X. Turon, Sublethal effects of contamination on

- the Mediterranean sponge *Crambe crambe*: Metal accumulation and biological responses, *Mar. Pollut. Bull.* 46 (2003) 1273–1284.
[https://doi.org/10.1016/S0025-326X\(03\)00190-5](https://doi.org/10.1016/S0025-326X(03)00190-5).
- [22] T. Perez, D. Longet, T. Schembri, P. Rebouillon, J. Vacelet, Effects of 12 years' operation of a sewage treatment plant on trace metal occurrence within a Mediterranean commercial sponge (*Spongia officinalis*, Demospongiae), *Mar. Pollut. Bull.* 50 (2005) 301–309.
<https://doi.org/10.1016/j.marpolbul.2004.11.001>.
- [23] J. Venkateswara Rao, K. Srikanth, R. Pallela, T. Gnaneshwar Rao, The use of marine sponge, *Haliclona tenuiramosa* as bioindicator to monitor heavy metal pollution in the coasts of Gulf of Mannar, India, *Environ. Monit. Assess.* 156 (2009) 451–459. <https://doi.org/10.1007/s10661-008-0497-x>.
- [24] J.V. Rao, P. Kavitha, K. Srikanth, P.K. Usman, T.G. Rao, Environmental contamination using accumulation of metals in marine sponge, *Sigmadocia fibulata* inhabiting the coastal waters of Gulf of Mannar, India, *Toxicol. Environ. Chem.* 89 (2007) 487–498. <https://doi.org/10.1080/02772240601150588>.
- [25] V. Padmaja, Sponges as Heavy Metal Accumulators and as Cytotoxic Agents, *J. Pharm.* 8 (2018) 49–56.
- [26] A.M. Orani, A. Barats, E. Vassileva, O.P. Thomas, Marine sponges as a powerful tool for trace elements biomonitoring studies in coastal environment, *Mar. Pollut. Bull.* 131 (2018) 633–645. <https://doi.org/10.1016/j.marpolbul.2018.04.073>.
- [27] C. Bauvais, S. Zirah, L. Piette, F. Chaspoul, I. Domart-Coulon, V. Chapon, P. Gallice, S. Rebuffat, T. Pérez, M.L. Bourguet-Kondracki, Spawning up metals: Bacteria associated with the marine sponge *Spongia officinalis*, *Mar. Environ.*

- Res. 104 (2015) 20–30. <https://doi.org/10.1016/j.marenvres.2014.12.005>.
- [28] J. Santos-Gandelman, M. Giambiagi-deMarval, W. Oelemann, M. Laport, Biotechnological Potential of Sponge-Associated Bacteria, *Curr. Pharm. Biotechnol.* 15 (2014) 143–155.
<https://doi.org/10.2174/1389201015666140711115033>.
- [29] J. Selvin, S. Shanmugha Priya, G. Seghal Kiran, T. Thangavelu, N. Sapna Bai, Sponge-associated marine bacteria as indicators of heavy metal pollution, *Microbiol. Res.* 164 (2009) 352–363.
<https://doi.org/10.1016/j.micres.2007.05.005>.
- [30] C. Longo, G. Corriero, M. Licciano, L. Stabili, Bacterial accumulation by the *Demospongiae Hymeniacidon perlevis*: A tool for the bioremediation of polluted seawater, *Mar. Pollut. Bull.* 60 (2010) 1182–1187.
<https://doi.org/10.1016/j.marpolbul.2010.03.035>.
- [31] H. Ehrlich, M. Wysokowski, S. Zóltowska-Aksamitowska, I. Petrenko, T. Jesionowski, Collagens of poriferan origin, *Mar. Drugs.* 16 (2018) 1–21.
<https://doi.org/10.3390/md16030079>.
- [32] R.J. Block, D. Bolling, The Amino Acid Composition of Keratins, *J. Biol. Chem.* 127 (1939) 685–694.
- [33] M. Norman, P. Bartczak, J. Zdarta, W. Tylus, T. Szatkowski, A.L. Stelling, H. Ehrlich, T. Jesionowski, Adsorption of C.I. natural red 4 onto spongin skeleton of marine demosponge, *Materials (Basel)*. 8 (2015) 96–116.
<https://doi.org/10.3390/ma8010096>.
- [34] M. Norman, J. Zdarta, P. Bartczak, A. Piasecki, I. Petrenko, H. Ehrlich, T. Jesionowski, Marine sponge skeleton photosensitized by copper phthalocyanine:

- A catalyst for Rhodamine B degradation, *Open Chem.* 14 (2016) 243–254.
<https://doi.org/10.1515/chem-2016-0025>.
- [35] M. Norman, S. Żółtowska-Aksamitowska, A. Zgoła-Grześkowiak, H. Ehrlich, T. Jesionowski, Iron(III) phthalocyanine supported on a spongin scaffold as an advanced photocatalyst in a highly efficient removal process of halophenols and bisphenol A, *J. Hazard. Mater.* 347 (2018) 78–88.
<https://doi.org/10.1016/j.jhazmat.2017.12.055>.
- [36] T. Szatkowski, K. Siwińska-Stefańska, M. Wysokowski, A. Stelling, Y. Joseph, H. Ehrlich, T. Jesionowski, Immobilization of Titanium(IV) Oxide onto 3D Spongin Scaffolds of Marine Sponge Origin According to Extreme Biomimetics Principles for Removal of C.I. Basic Blue 9, *Biomimetics.* 2 (2017) 4.
<https://doi.org/10.3390/biomimetics2020004>.
- [37] M. Norman, P. Bartczak, J. Zdarta, H. Ehrlich, T. Jesionowski, Anthocyanin dye conjugated with *Hippospongia communis* marine demosponge skeleton and its antiradical activity, *Dye. Pigment.* 134 (2016) 541–552.
<https://doi.org/10.1016/j.dyepig.2016.08.019>.
- [38] M. Norman, P. Bartczak, J. Zdarta, W. Tomala, B. Żurańska, A. Dobrowolska, A. Piasecki, K. Czaczyk, H. Ehrlich, T. Jesionowski, Sodium copper chlorophyllin immobilization onto *Hippospongia communis* marine demosponge skeleton and its antibacterial activity, *Int. J. Mol. Sci.* 17 (2016).
<https://doi.org/10.3390/ijms17101564>.
- [39] D. Wang, J. Song, S. Lin, J. Wen, C. Ma, Y. Yuan, M. Lei, X. Wang, N. Wang, H. Wu, A Marine-Inspired Hybrid Sponge for Highly Efficient Uranium Extraction from Seawater, *Adv. Funct. Mater.* 29 (2019) 1–12.

- <https://doi.org/10.1002/adfm.201901009>.
- [40] J. Zdarta, K. Anteck, R. Frankowski, A. Zgoła-Grzeskowiak, H. Ehrlich, T. Jesionowski, The effect of operational parameters on the biodegradation of bisphenols by *Trametes versicolor* laccase immobilized on *Hippospongia communis* spongin scaffolds, *Sci. Total Environ.* 615 (2018) 784–795. <https://doi.org/10.1016/j.scitotenv.2017.09.213>.
- [41] V. Ashouri, M. Rahimi-Nasrabadi, G. Attaran Fariman, K. Adib, M.M. Zahedi, M.R. Ganjali, E. Marzi Khosrowshahi, Extraction and pre-concentration of ketamine by using a three-dimensional spongin-based scaffold of the *Haliclona* sp. marine demosponge origin, *Appl. Phys. A Mater. Sci. Process.* 126 (2020) 1–12. <https://doi.org/10.1007/s00339-020-03598-z>.
- [42] T. Szatkowski, M. Wysokowski, G. Lota, D. Peziak, V. V. Bazhenov, G. Nowaczyk, J. Walter, S.L. Molodtsov, H. Stöcker, C. Himcinschi, I. Petrenko, A.L. Stelling, S. Jurga, T. Jesionowski, H. Ehrlich, Novel nanostructured hematite–spongin composite developed using an extreme biomimetic approach, *RSC Adv.* 5 (2015) 79031–79040. <https://doi.org/10.1039/c5ra09379a>.
- [43] T. Szatkowski, K. Kopczyński, M. Motylenko, H. Borrmann, B. Mania, M. Graś, G. Lota, V. V. Bazhenov, D. Rafaja, F. Roth, J. Weise, E. Langer, M. Wysokowski, S. Żółtowska-Aksamitowska, I. Petrenko, S.L. Molodtsov, J. Hubálková, C.G. Aneziris, Y. Joseph, A.L. Stelling, H. Ehrlich, T. Jesionowski, Extreme biomimetics: A carbonized 3D spongin scaffold as a novel support for nanostructured manganese oxide(IV) and its electrochemical applications, *Nano Res.* 11 (2018) 4199–4214. <https://doi.org/10.1007/s12274-018-2008-x>.
- [44] I. Petrenko, A.P. Summers, P. Simon, S. Żółtowska-Aksamitowska, M.

- Motylenko, C. Schimpf, D. Rafaja, F. Roth, K. Kummer, E. Brendler, O.S. Pokrovsky, R. Galli, M. Wysokowski, H. Meissner, E. Niederschlag, Y. Joseph, S. Molodtsov, A. Ereskovsky, V. Sivkov, S. Nekipelov, O. Petrova, O. Volkova, M. Bertau, M. Kraft, A. Rogalev, M. Kopani, T. Jesionowski, H. Ehrlich, Extreme biomimetics: Preservation of molecular detail in centimeter-scale samples of biological meshes laid down by sponges, *Sci. Adv.* 5 (2019) 1–12. <https://doi.org/10.1126/sciadv.aax2805>.
- [45] D. Tsurkan, M. Wysokowski, I. Petrenko, A. Voronkina, Y. Khrunyk, A. Fursov, H. Ehrlich, Modern scaffolding strategies based on naturally pre-fabricated 3D biomaterials of poriferan origin, *Appl. Phys. A Mater. Sci. Process.* 126 (2020) 1–9. <https://doi.org/10.1007/s00339-020-03564-9>.
- [46] S. Sharma, A. Yadav, Marine sponge derived cyclic peptides for removal of mercury, *Asian J. Chem.* 30 (2018) 1873–1880. <https://doi.org/10.14233/ajchem.2018.21356>.
- [47] V.K. Mubiana, R. Blust, Effects of temperature on scope for growth and accumulation of Cd, Co, Cu and Pb by the marine bivalve *Mytilus edulis*, *Mar. Environ. Res.* 63 (2007) 219–235. <https://doi.org/10.1016/j.marenvres.2006.08.005>.
- [48] B. Henriques, F. Coppola, R. Monteiro, J. Pinto, T. Viana, C. Pretti, A. Soares, R. Freitas, E. Pereira, Toxicological assessment of anthropogenic Gadolinium in seawater: Biochemical effects in mussels *Mytilus galloprovincialis*, *Sci. Total Environ.* 664 (2019) 626–634. <https://doi.org/10.1016/j.scitotenv.2019.01.341>.
- [49] F. Coppola, D.S. Tavares, B. Henriques, R. Monteiro, T. Trindade, E. Figueira, A.M.V.M. Soares, E. Pereira, R. Freitas, Can water remediated by manganese

- spinel ferrite nanoparticles be safe for marine bivalves?, *Sci. Total Environ.* (2020) 108197. <https://doi.org/10.1016/j.matdes.2019.108197>.
- [50] M.J. Atkinson, C. Bingman, P.O. Box, C. Bingman, P.O. Box, Elemental composition of commercial seasalts, *J. Aquaric. Aquat. Sci.* VIII (1997) 39–43. <http://www.rudyv.be/Aquarium/sels.pdf>.
- [51] B. Henriques, G. Gonçalves, N. Emami, E. Pereira, M. Vila, P.A.A.P. Marques, Optimized graphene oxide foam with enhanced performance and high selectivity for mercury removal from water, *J. Hazard. Mater.* 301 (2016) 453–461. <https://doi.org/10.1016/j.jhazmat.2015.09.028>.
- [52] M.I. El-Khaiary, G.F. Malash, Common data analysis errors in batch adsorption studies, *Hydrometallurgy.* 105 (2011) 314–320. <https://doi.org/DOI 10.1016/j.hydromet.2010.11.005>.
- [53] S. Lagergren, About the theory of so-called adsorption of soluble substances, *K. Sven Vetén Hand.* 24 (1898) 1–39.
- [54] Y.S. Ho, G. McKay, Pseudo-second order model for sorption processes, *Process Biochem.* 34 (1999) 451–465. [https://doi.org/Doi 10.1016/S0032-9592\(98\)00112-5](https://doi.org/Doi 10.1016/S0032-9592(98)00112-5).
- [55] M.J.D. Low, Kinetics of Chemisorption of Gases on Solids, *Chem. Rev.* 60 (1960) 267–312. <https://doi.org/Doi 10.1021/Cr60205a003>.
- [56] G.E. Boyd, A.W. Adamson, L.S. Myers, The Exchange Adsorption of Ions from Aqueous Solutions by Organic Zeolites .2., *J. Am. Chem. Soc.* 69 (1947) 2836–2848. <https://doi.org/Doi 10.1021/Ja01203a066>.
- [57] W.J. Weber, J.C. Morris, Kinetics of adsorption on carbon from solution, *Kinet. Adsorpt. Carbon from Solut.* (1963).

- [58] O. Hamdaoui, E. Naffrechoux, Modeling of adsorption isotherms of phenol and chlorophenols onto granular activated carbon. Part I. Two-parameter models and equations allowing determination of thermodynamic parameters, *J. Hazard. Mater.* 147 (2007) 381–394. <https://doi.org/10.1016/j.jhazmat.2007.01.021>.
- [59] I. Langmuir, The Adsorption of Gases on Plane Surfaces of Mica, *J. Am. Chem. Soc.* 40 (1918) 1361–1403. <https://doi.org/10.1021/ja01269a066>.
- [60] Q. Hu, Z. Zhang, Application of Dubinin–Radushkevich isotherm model at the solid/solution interface: A theoretical analysis, *J. Mol. Liq.* 277 (2019) 646–648. <https://doi.org/10.1016/j.molliq.2019.01.005>.
- [61] R. Sips, On the structure of a catalyst surface, *J. Chem. Phys.* 16 (1948) 490–495. <https://doi.org/10.1063/1.1746922>.
- [62] C.T. Costley, K.F. Mossop, J.R. Dean, L.M. Garden, J. Marshall, J. Carroll, Determination of mercury in environmental and biological samples using pyrolysis atomic absorption spectrometry with gold amalgamation, *Anal. Chim. Acta.* 405 (2000) 179–183. [https://doi.org/10.1016/S0003-2670\(99\)00742-4](https://doi.org/10.1016/S0003-2670(99)00742-4).
- [63] W. Zhang, X.J. Luo, L.N. Niu, H.Y. Yang, C.K.Y. Yiu, T. Da Wang, L.Q. Zhou, J. Mao, C. Huang, D.H. Pashley, F.R. Tay, Biomimetic intrafibrillar mineralization of type I collagen with intermediate precursors-loaded mesoporous carriers, *Sci. Rep.* 5 (2015) 1–11. <https://doi.org/10.1038/srep11199>.
- [64] M. Norman, M. Sc, Skeletons of selected marine demosponges as supports for dyes adsorption, Poznan University of Technology, 2017.
- [65] B. Janković, L. Kolar-Anić, I. Smičiklas, S. Dimović, D. Arandelović, The non-isothermal thermogravimetric tests of animal bones combustion. Part. I. Kinetic analysis, *Thermochim. Acta.* 495 (2009) 129–138.

- <https://doi.org/10.1016/j.tca.2009.06.016>.
- [66] Council of the European Union, E. Parliament, Directive 2013/39/EU of the European Parliament and of the Council of 12 August 2013 amending Directives 2000/60/EC and 2008/105/EC as regards priority substances in the field of water policy, Official Journal of the European Union, 2013.
- [67] A. Bessa, B. Henriques, G. Gonçalves, G. Irueta, E. Pereira, P.A.A.P. Marques, Graphene oxide/polyethyleneimine aerogel for high-performance mercury sorption from natural waters, *Chem. Eng. J.* 398 (2020) 125587.
<https://doi.org/10.1016/j.cej.2020.125587>.
- [68] G.F. Malash, M.I. El-Khaiary, Piecewise linear regression: A statistical method for the analysis of experimental adsorption data by the intraparticle-diffusion models, *Chem. Eng. J.* 163 (2010) 256–263.
<https://doi.org/10.1016/j.cej.2010.07.059>.
- [69] C.W. Cheung, J.F. Porter, G. McKay, Sorption kinetics for the removal of copper and zinc from effluents using bone char, *Sep. Purif. Technol.* 19 (2000) 55–64.
[https://doi.org/10.1016/S1383-5866\(99\)00073-8](https://doi.org/10.1016/S1383-5866(99)00073-8).
- [70] H. Qiu, L. Lv, B. Pan, Q. Zhang, W. Zhang, Q. Zhang, Critical review in adsorption kinetic models, *J. Zhejiang Univ. Sci. A.* 10 (2009) 716–724.
<https://doi.org/10.1631/jzus.A0820524>.
- [71] L.S. Rocha, C.B. Lopes, J.A. Borges, A.C. Duarte, E. Pereira, Valuation of Unmodified Rice Husk Waste as an Eco-Friendly Sorbent to Remove Mercury: A Study Using Environmental Realistic Concentrations, *Water. Air. Soil Pollut.* 224 (2013). <https://doi.org/10.1007/s11270-013-1599-9>.
- [72] A. Bessa, G. Gonçalves, B. Henriques, E.M. Domingues, E. Pereira, P.A.A.P.

Marques, Green Graphene–Chitosan Sorbent Materials for Mercury Water Remediation, *Nanomaterials*. 10 (2020) 1474.

<https://doi.org/10.3390/nano10081474>.

[73] A. Günay, E. Arslankaya, I. Tosun, Lead removal from aqueous solution by natural and pretreated clinoptilolite: Adsorption equilibrium and kinetics, *J. Hazard. Mater.* 146 (2007) 362–371.

<https://doi.org/10.1016/j.jhazmat.2006.12.034>.

Graphical abstract



Credit Author statement

Eddy M. Domingues: Conceptualization, Formal Analysis, Investigation, Writing - Original Draft, Writing – Reviewing and Editing, Visualization

Gil Gonçalves: Conceptualization, Investigation, Writing – Reviewing and Editing

Bruno Henriques: Formal analysis, Writing – Reviewing and Editing

Eduarda Pereira: Resources, Writing – Reviewing and Editing, Funding Acquisition

Paula A. A. P. Marques: Conceptualization, Resources, Writing – Reviewing and Editing, Supervision, Project administration, Funding Acquisition

Journal Pre-proof

Declaration of interests

The authors declare that they have no known competing financial interests or personal relationships that could have appeared to influence the work reported in this paper.

The authors declare the following financial interests/personal relationships which may be considered as potential competing interests:

Journal Pre-proof

Highlights

- Pure marine sponge was tested as sorbent for Hg(II) removal in real waters.
- Up to 89% Hg(II) removal from seawater using 40 mg L⁻¹ of marine sponge.
- Pseudo-second order kinetic model is the best fit for the experimental data.
- Marine sponge samples could be regenerated and reused up to three times.

Journal Pre-proof